



Fretting wear and electrochemical corrosion of well-adhered CVD diamond films deposited on steel substrates with a WC–Co interlayer

Qiu-ping Wei^{a,b,c}, Z.M. Yu^{a,*}, Michael N.R. Ashfold^b, L. Ma^c, Zhong Chen^a

^a School of Materials Science and Engineering, Central South University, Changsha, 410083, PR China

^b School of Chemistry, University of Bristol, Bristol BS8 1TS, United Kingdom

^c State Key Laboratory of Powder Metallurgy, Central South University, Changsha, 410083, PR China

ARTICLE INFO

Article history:

Received 8 February 2010

Received in revised form 26 March 2010

Accepted 20 April 2010

Available online 27 April 2010

Keywords:

CVD diamond films

Steel substrates

Fretting wear

Corrosion potential

ABSTRACT

Diamond films have been grown on carbon steel substrates by hot-filament chemical vapour deposition methods. A Co-containing tungsten-carbide (WC–Co) coating prepared by high velocity oxy-fuel spraying was used as an intermediate layer on the steel substrates to minimize the early formation of graphite (and thus growth of low quality diamond films) and to enhance the diamond film adhesion. The effects of the WC–Co interlayer on nucleation, quality, adhesion, tribological behaviour and electrochemical corrosion of the diamond film were investigated. The diamond films exhibit excellent adhesion under Rockwell indentation testing (1500 N load) and when subjected to high-speed, high-load, long-time reciprocating dry sliding ball-on-flat wear tests against a Si₃N₄ counterface in ambient air (500 rpm, 200 N, 300,000 cycles). A WC–Co interlayer with appropriate chemical pretreatment is shown to play an important role in improving the nucleation, quality and adhesion of the diamond film, relative to that shown by substrates without such pretreatment.

© 2010 Elsevier B.V. All rights reserved.

1. Introduction

As engineering applications become ever more demanding, there is an increasing requirement for composite coatings that protect the substrate so as to retain its mechanical strength, but also enhance the resistance of the substrate to wear and corrosion. Alloy steels are among the most commonly used and cost-effective structural materials in modern industry. However, when steel is used for critical wear resistant components and machining tools in harsh (wear, corrosive and erosive) environments, accelerated damage usually occurs. Diamond possesses many unique properties (e.g. the highest hardness and wear resistance, the lowest friction coefficient, as well as chemical inertness to acidic, alkaline and saline media), which make diamond films grown by chemical vapour deposition (CVD) potentially ideal coatings for wear resistant components and machining applications [1,2]. Well-adhered diamond films deposited on steel surfaces can lead to major improvements in the life and performance of steel tools, since the early failure of such tools is usually initiated at the outermost surface. Despite the great industrial potential, practical applications of this technique have been limited due to difficulties in achieving satisfactory diamond film adhesion to the steels, as a result of several limiting factors [3–5]. These include: (1) iron catalyses graphite formation at diamond/steel interfaces during the CVD process [6,7]; (2) the high solubility of carbon in the iron fcc phase leads to prolonged diamond nucleation times [8,9];

(3) the large difference in the coefficients of thermal expansion between diamond and steel may induce high stress within the deposited diamond films [9]. As direct diamond coating of steel is very difficult, modification of the surface, or the use of interlayers, in order to improve the quality and adhesion of any diamond coating is indispensable. Different kinds of steel substrate modifications [10–12], and the application of various interlayers [9,12–15] have been reported, but the breakthroughs described to date are not yet sufficient to satisfy the demands of most technical applications.

In this work, a Co-containing tungsten-carbide (WC–Co) coating has been deposited on carbon steel using a high velocity oxy-fuel (HVOF) thermal spray technique to act as an intermediate layer prior to diamond film deposition, in order to improve the quality and adhesion of the latter. The use of intermediate layers involves complex and costly multi-step procedures, and the adhesion at both the substrate/interlayer and the interlayer/diamond interfaces has to be simultaneously guaranteed. WC–Co coatings were selected as the interlayer after due consideration of the following: (a) cemented carbides (WC–Co) are successfully used as substrates in the material forming industry, and CVD diamond films deposited on WC–Co components and tools are already available in the market; (b) thermally sprayed WC–Co coatings are now used extensively in a variety of tribological, corrosion and tribo-corrosion applications [16]; (c) sliding contact between ductile materials often induces large plastic strains in the near-surface regions, and accumulated plastic strain at the coating/substrate interface can lead to film breakdown [10]. The interposition of a hard, thick WC–Co coating between the ductile steel substrate and a thin diamond film should reduce any plastic strain in the near-surface regions induced by

* Corresponding author. Tel.: +86 731 8830335; fax: +86 731 8876692.
E-mail address: zhiming@mail.csu.edu.cn (Z.M. Yu).

sliding contact. Further, the cost of obtaining a thick WC–Co interlayer by HVOF is lower than that of other interlayers deposited by physical vapour deposition (PVD) technology; (d) tungsten-carbide interlayers have a low thermal expansion coefficient (relative to many other interlayers), which should be beneficial in reducing the mismatch between the thermal expansion coefficients of diamond and the substrate; (e) tungsten can form a carbide, which can be expected to encourage nucleation of diamond seed crystals [17,18].

2. Experimental details

Diamond films were deposited in a hot-filament-assisted chemical vapour deposition (HFCVD) reactor, as described previously [19]. The films were grown on AISI 1085 carbon steel plates, and a WC–Co coating was used as an interlayer to improve the nucleation, quality and adhesion of the diamond film. The flat specimens used in this study were $50 \times 30 \times 5 \text{ mm}^3$ AISI 1085 carbon steel plates coated with a WC–Co interlayer ($\sim 400 \mu\text{m}$ in thickness) by HVOF. The WC–Co blends used here typically comprised 85–90% WC and 10–15% Co powder (powder size $\sim 2\text{--}5 \mu\text{m}$), and the spraying parameters were: oxygen flow 2000 scfh; spray distance 30 cm; fuel rate 6.0 gph. The substrates were then cut into smaller plates of dimension $10 \times 10 \times 5 \text{ mm}^3$ by spark cutting. Due to the high roughness of the sprayed WC–Co interlayer, the specimens were polished with diamond polishing agent; the final interlayer thickness after polishing was $\sim 200 \mu\text{m}$ and the surface roughness $< 3 \mu\text{m}$. Selected specimens (all of which will henceforth be termed B specimens) were then etched using the following two-step pretreatment: (i) etching by Murakami's reagent (10 g $\text{K}_3[\text{Fe}(\text{CN})_6]$ + 10 g KOH + 100 ml H_2O) for 3 min in an ultrasonic vessel; (ii) removal of the surface Co by etching in an acidic solution of hydrogen peroxide (2 ml 96 wt.% H_2SO_4 + 2 ml 68 wt.% HNO_3 + 20 ml 40% w/v H_2O_2 + 40 ml H_2O) for 2 min. Prior to deposition, all of these pretreated B specimens were first abraded ultrasonically in a suspension of diamond powder ($< 500 \text{ nm}$ particle size) in acetone for 30 min. This treatment is often referred to as 'seeding', which encourages the subsequent inhomogeneous nucleation of diamond during CVD – either by implanting ultrafine diamond fragments into the substrate surface, or by creating suitable defects on the substrate surface [2]. Table 1 shows the CVD parameters used, which were typically held constant for each specimen and deposition. Five specimens were deposited under the conditions termed A, and ten specimens deposited using conditions B. The results presented in this article are representative of those found for all specimens subjected to a given parameter set.

Specimens were characterized by a variety of techniques, including scanning electron microscopy (SEM, FEI, Sirion200 Field-emission SEM and Quanta200 Environmental SEM), X-ray diffraction (XRD: Dmax-2500VBX using $\text{Cu K}\alpha$ radiation at a wavelength of 0.154 nm), energy dispersive X-ray analysis (EDX: EDAX model) and Raman spectroscopy (LabRAM HR800). Raman spectra were measured with an argon ion laser operating at 488 nm with an output power of 100 mW. The cross-sections of the specimens after indentation testing were obtained by polishing them with diamond abrasive paste and subsequently ultrasonic etching in Murakami solution for 1 min.

Table 1
Experimental parameters used for diamond film deposition on carbon steel substrates with a WC–Co interlayer.

Specimen type	A	B
Substrate pretreatment	No	Two-step pretreatment
Filament–substrate distance (mm)	8 ± 2	8 ± 2
Substrate temperature ($^\circ\text{C}$)	750 ± 50	750 ± 50
CH_4/H_2 (vol.%)	2	3
Deposition pressure (kPa)	3	3
Total gas flow rate (sccm)	50	50
Deposition time (min)	420	480

Electrochemical investigations of the diamond-coated steel specimens were conducted in a glass cell with a platinum counter electrode and a saturated calomel electrode (SCE) as reference using a galvanostat/potentiostat. Chronopotentiometry with a current density of $700 \text{ mA}/\text{cm}^2$ was performed at a CHI660C/CHI680 electrochemical work station. The specimens were tested in 3.5 mol/l aqueous NaCl solutions at room temperature. The open circuit potential curves were measured after immersing the coated layers in the solution for 30 min to ensure potential stabilization. The potentiodynamic polarisation curves were recorded at a scan rate of $1.0 \text{ mV}/\text{s}$, in both the forward and reverse directions, starting from cathodic potentials. For all specimens, only the diamond-coated top surfaces were exposed to the solution; the other faces (including the backsides) were shielded by a corrosion resistant lacquer. The current densities were thus obtained by dividing the measured currents by the surface areas that were actually exposed to the solution.

The adhesion and tribological properties of the diamond-coated steel substrates were characterized using a Rockwell hardness tester with a Brale diamond indenter (angle = 120° , radius = 0.2 mm) at loads of 600 N, 1000 N and 1500 N, respectively, and by reciprocating fretting tests. Friction and wear tests were conducted using a ball-on-disk tribometer with pairs of silicon nitride (Si_3N_4) balls and diamond-coated substrates. The measurements were made in open air, at ambient temperature and at a relative humidity (RH) of $(65 \pm 5)\%$. A Si_3N_4 ball (9.5 mm in diameter) with a surface finish of better than $0.1 \mu\text{m}$ was loaded on top of the diamond-coated flat steel specimen as counterface materials mounted on a horizontal translation table. A large load of 200 N was applied to the Si_3N_4 ball, while the test specimens were

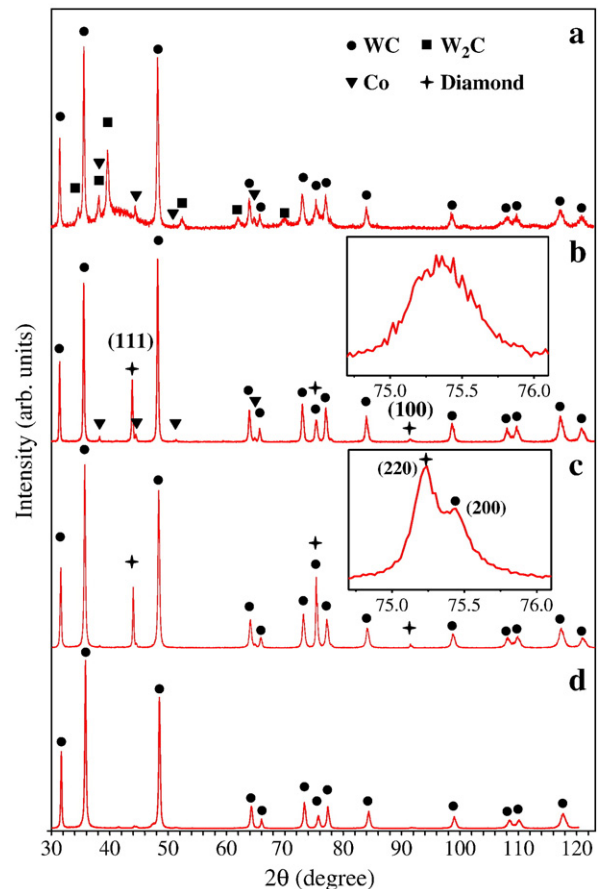


Fig. 1. X-ray diffraction patterns of (a) the as-coated WC–Co interlayer on carbon steel substrate, (b) an example of specimen A, (c) a specimen B sample, and (d) the bulk sintered WC–13 wt.%Co plate.

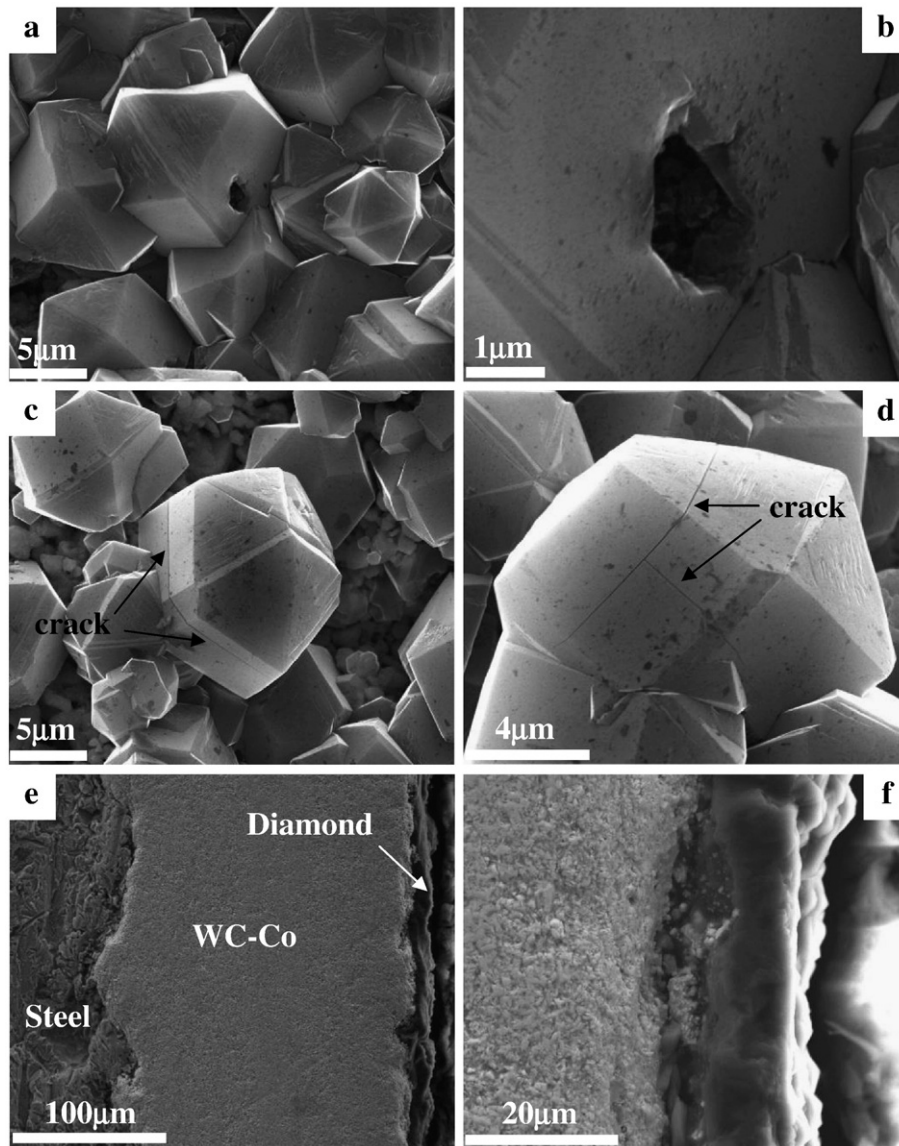


Fig. 2. Representative SEM images of diamond films deposited on an A specimen. Images (a)–(d) are top views, while (e) and (f) are cross-sections.

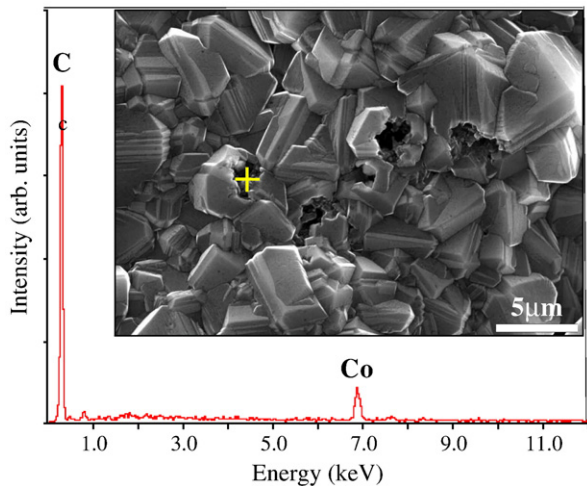


Fig. 3. EDX analysis of an obvious defect region (indicated on the image with a +) in a diamond film deposited on an A specimen.

subjected to a reciprocating displacement. The sliding velocity was set at 500 rpm (≈ 8.33 Hz). The coefficient of friction (COF) was obtained from the measurement of the tangential force exerted on the ball during sliding. The COF signal was integrated with a time constant of 0.01 s.

3. Results

3.1. X-ray diffraction studies

XRD patterns of the as-coated WC–Co interlayer on a carbon steel substrate, of CVD diamond films on A and B specimens, and of a bulk sintered WC–13 wt.%Co plate, are shown in Fig. 1 (a), (b), (c) and (d), respectively. As Fig. 1 (a) shows, the surface of the carbon steel substrate with a WC–Co interlayer is comprised mainly of WC, W_2C , and Co binder phases. The XRD patterns of the diamond films deposited on carbon steel substrates with a WC–Co interlayer (Fig. 1 (b) and (c)) both reveal an obvious phase transformation. The diffuse scattered background clearly decreases, and the crystallinity improves. Most of the W_2C phase has disappeared, and the major constituent is the WC phase. The XRD pattern of specimen B is very similar to that of the bulk sintered

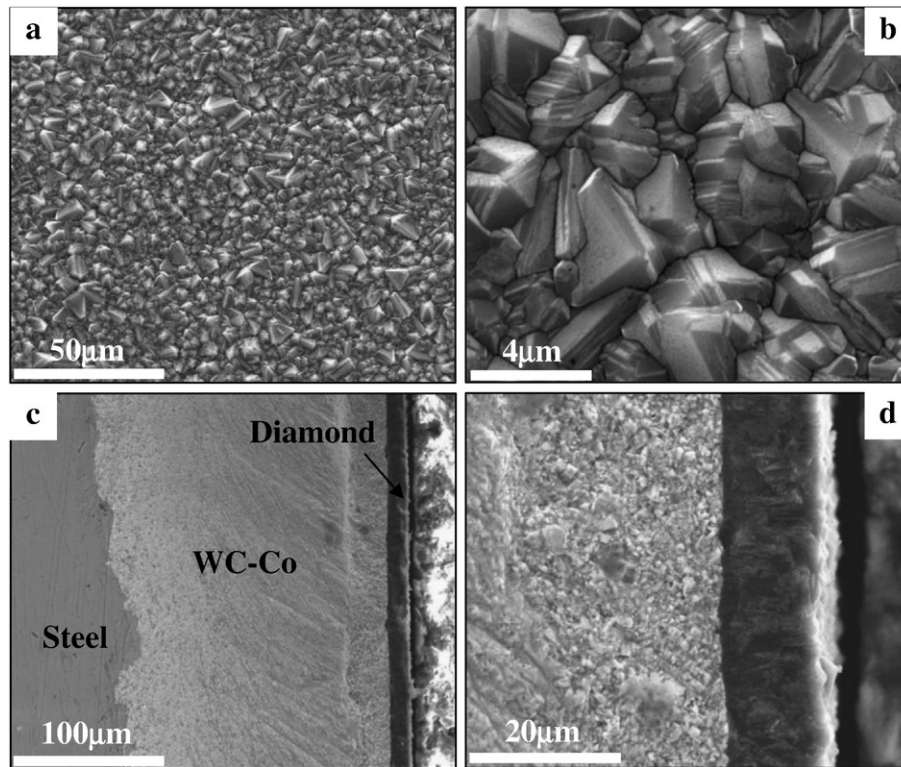


Fig. 4. SEM images of a diamond film deposited on a B specimen. Images (a) and (b) are top views, while images (c) and (d) show cross-sections, each displayed at two different magnifications.

WC-13 wt.%Co plate (see Fig. 1 (c) and (d)). The XRD results are consistent with the view that, during diamond growth by HFCVD, diffusion of active atomic carbon results in a composite interlayer of WC, with the W_2C phase transforming into a WC dominated layer [18] by a reaction that can be written as



Cobalt peaks are obvious in the XRD spectrum shown in Fig. 1 (b). The XRD patterns of Fig. 1 (b) and (c) both indicate the presence of diamond. Peaks at 2θ diffraction angles of 44.0° , 75.2° and 91.4° are clearly evident, and correspond to, respectively, the (111), (220) and (311) reflections of the cubic diamond structure. Note that the peak in the range $2\theta \sim 75.4^\circ$ matches closely with the diamond (220) peak at 75.302° and the WC (200) peak at 75.477° . We therefore assign this peak to overlapping diamond (220) and WC (200) peaks. This blended feature has been deconvoluted and analysed after expansion (shown in the insets to Fig. 1 (b) and (c)). Information regarding the texture of the diamond films can be obtained by comparing the diffraction intensity with the ASTM (American Society for Testing and Materials) data. The $I_{(220)}/I_{(111)}$, $I_{(311)}/I_{(111)}$, $I_{(331)}/I_{(111)}$ and $I_{(400)}/I_{(111)}$ intensity ratios were compared with the relative peak intensities measured for a B sample. The large $I_{(220)}/I_{(111)}$ ratio indicates preferred $\langle 110 \rangle$ textured growth of this diamond film [20].

3.2. Investigation of surface and cross-section morphology

Fig. 2 shows representative surface and cross-section SEM images of diamond films deposited on an A specimen. The surface images reveal that the diamond coating has nucleated very non-uniformly, but that the individual crystallites show typical diamond crystal morphologies. Many of the diamond crystallites appear 'moth-eaten', as illustrated in Fig. 2 (a) and (b); the core of the crystallite has a hole. Cobalt can be detected in the hole by EDX, but not tungsten (see Fig. 3). Fault lines

('cracks') are also visible on the surfaces of some of the diamond crystals (Fig. 2 (c) and (d)). Donnet et al. [21] showed that cobalt diffuses during the nucleation and growth of diamond on WC-Co substrates, and can influence the structure and quality of the diamond coating. At high substrate temperature, $T_s > 800^\circ C$, ball-shape particles of cobalt, with diameters $\sim 0.7 \mu m$, were observed on the top surface of thick ($> 50 \mu m$) diamond coatings. Even at relatively low substrate temperatures ($T_s \sim 550^\circ C$), cobalt dissolution in the carbon film was detected by EDX. We are not aware of any previous reports of as-grown diamond crystallites exhibiting damage such as that shown here. The cross-section images clearly show a continuous tri-layer structure, with a central WC-Co interlayer (thickness $\sim 200 \mu m$) and a rugged, $< 20 \mu m$ thick diamond film at the surface.

The surface and cross-sectional morphologies of diamond films deposited on B specimens were also investigated by SEM (Fig. 4). The surface SEM images show a dense and homogeneous diamond coating, with no obvious defects, and typical diamond crystallite morphologies (Fig. 4 (a), (b)). The magnified images highlight the rough surface finish (Fig. 4(b)) and the coarse columnar morphology (Fig. 4(d)) – typical of most polycrystalline diamond films grown from dilute CH_4/H_2 gas mixtures. No ball-shape cobalt particles, nor any damaged diamond crystallites, are evident on the diamond film surface. The cross-section images again show a continuous tri-layer structure with a central $\sim 200 \mu m$ thick WC-Co interlayer and the diamond film (thickness $< 20 \mu m$) at the surface.

3.3. Laser Raman analysis

The Raman spectra for the films deposited on specimens A and B are shown in Fig. 5. The diamond film deposited on an A sample shows a relatively wide peak in the wavenumber range $1330\text{--}1345 \text{ cm}^{-1}$, whereas films deposited on B specimens display a sharp peak centered at 1336.4 cm^{-1} . Given their comparatively narrow widths and their intensities, we conclude that these peaks are both associated with

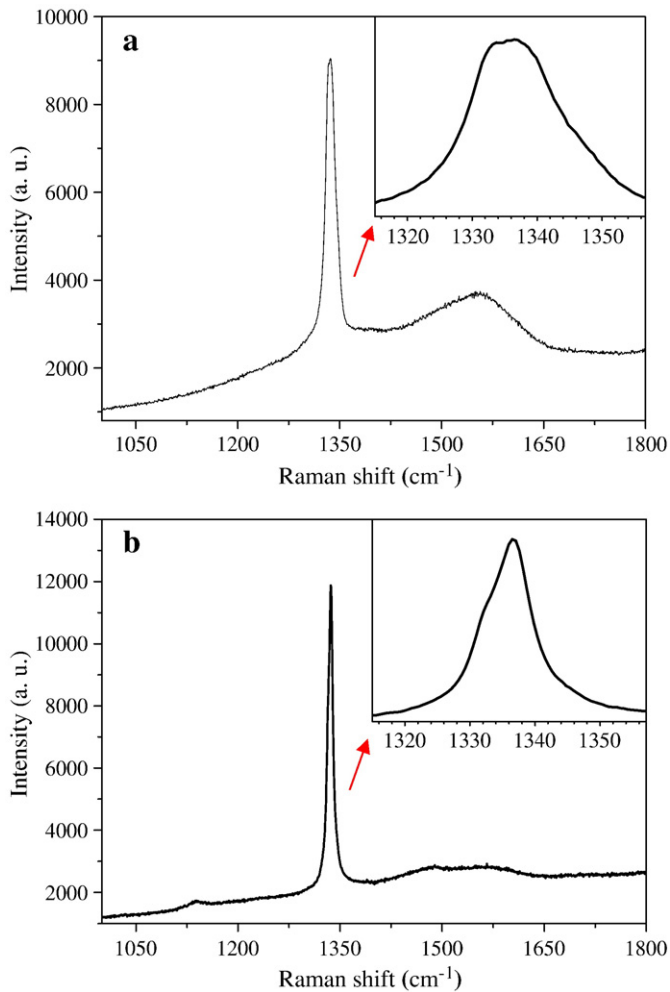


Fig. 5. Raman spectra of diamond films deposited on (a) A and (b) B specimens. The insets show expanded views of the $\sim 1340\text{ cm}^{-1}$ feature.

diamond. Raman signals from graphitic (sp^2 -bonded) carbon in the range of $1500\text{--}1600\text{ cm}^{-1}$ can also be observed in both spectra. The intensity ratio between the sp^2 characteristic feature at $\sim 1550\text{ cm}^{-1}$ and the diamond peak at $\sim 1340\text{ cm}^{-1}$ is larger for the film deposited on the A specimen than that for specimen B, consistent with a reduction of the relative amount of sp^2 -bonded carbon and an increase in the quality of the diamond films deposited on WC–Co coated carbon steel after the two-step pretreatment. This observation also confirms the effectiveness of the two-step chemical pretreatment process in minimizing catalytically enhanced deposition (by Co) of non-diamond (sp^2 -bonded) carbon phases. The diamond peaks in the measured Raman spectra are somewhat blue-shifted with respect to the peak position in a natural, stress-free diamond sample (1332.2 cm^{-1}), which might be the result of residual, compressive stress, possibly attributable to the mismatch in thermal expansion between the substrate and diamond films [22]. Following diamond growth for long times (480 min), the diamond film stress may vary with distance from the substrate, due to the different time of nucleation and growth, which will tend to result in broader diamond Raman peaks in the range of $1330\text{--}1340\text{ cm}^{-1}$, as seen in Fig. 5.

3.4. Indentation testing

In order to analyse the influence of the WC–Co interlayer and the residual stresses acting on the polycrystalline diamond film deposited on specimens A and B, Rockwell indentation tests were performed

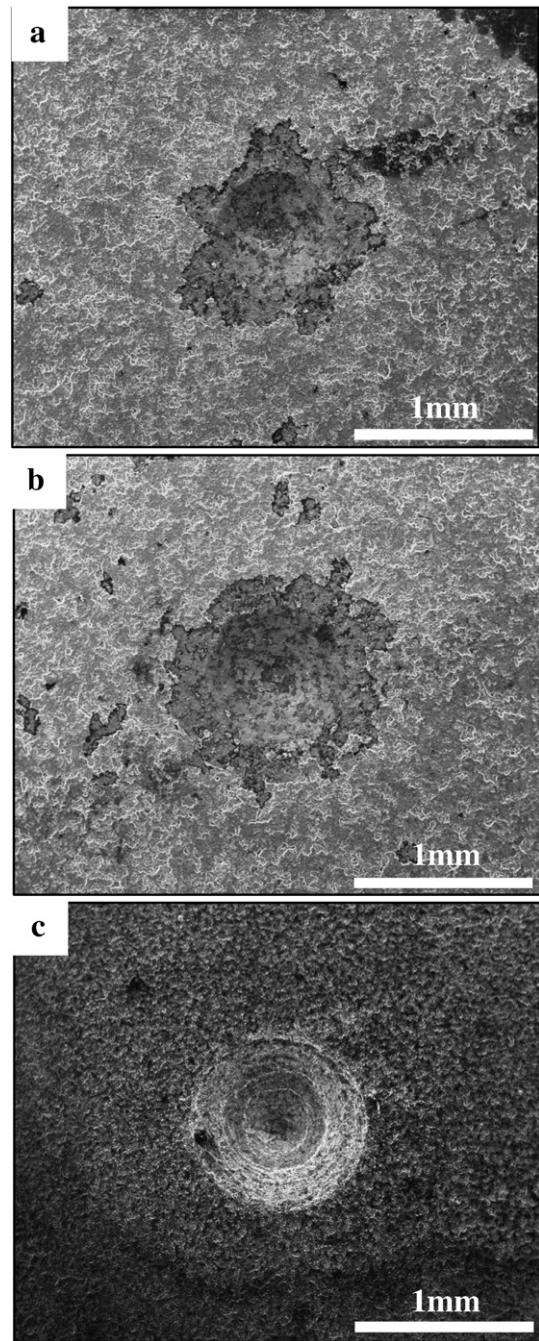


Fig. 6. SEM images of Rockwell indentations on A specimens under loads of (a) 600 N and (b) 1000 N, and of a B specimen under a load of (c) 1500 N.

with various loads (Fig. 6). Large scale flaking-off is evident around both indentations on the A specimen, but no flaking or cracking is evident around the indentation on specimen B. Such findings are consistent with the cross-section results shown in Figs. 2 and 4.

3.5. Electrochemical behaviour of diamond-coated specimens

Fig. 7 shows the electrochemical behaviour of the base carbon steel substrate, the steel substrate coated with the WC–Co interlayer, and a diamond film deposited on a B specimen, upon potentiodynamic polarisation in an aerated 3.5 mol/l NaCl solution. The potential corresponding to the minimum current density is known as the

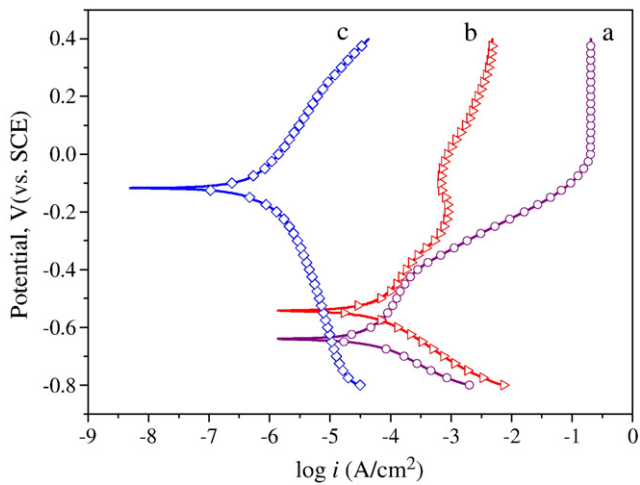


Fig. 7. Comparison of potentiodynamic polarization curves of: (a) the carbon steel substrate; (b) the WC–Co interlayer coated carbon steel substrate; and (c) a diamond film deposited on specimen B, in the aerated 3.5 mol/l NaCl solution.

equilibrium corrosion potential (E_{corr}). Compared to the bare carbon steel reference specimen, E_{corr} is shifted in the positive direction for both the WC–Co interlayer coated carbon steel substrate and the diamond-coated specimen B; the magnitude of this shift for the diamond-coated carbon steel substrate with a WC–Co interlayer is much greater, however. An SEM micrograph of the surface of a diamond-coated B specimen subjected to anodic polarisation is presented in Fig. 8. No evidence of attack or morphological changes of the diamond film are observable after anodic polarisation for 30 min.

3.6. Tribological behaviour of diamond-coated specimens

Fig. 9 shows the COFs of Si_3N_4 balls sliding in air against diamond films on specimen A and on B specimens both before (B_1) and after (B_2) electrochemical investigation. The initial COF of the diamond film deposited on specimen A against Si_3N_4 is higher (0.36) than that of films deposited on specimen B measured both before (0.05, B_1) and after (0.11, B_2) electrochemical investigation. The COF of the diamond film deposited on the A specimen against Si_3N_4 , after engaging the load stabilization period, decreases slightly and then remains at a very high level (0.35) (see Fig. 9 (a)). Comparison with the results for the B_1 and B_2 specimens indicates that the diamond film on specimen A

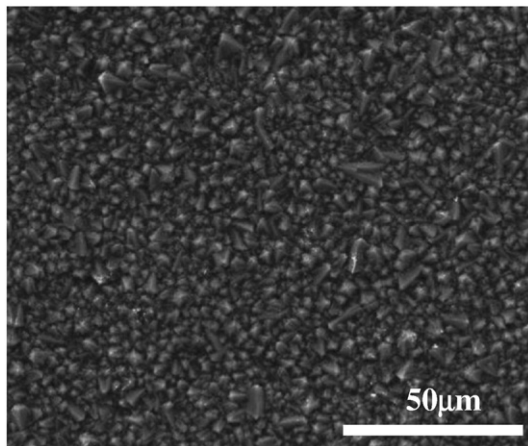


Fig. 8. Micrograph illustrating the surface morphology of the diamond film deposited on a B specimen after 30 min immersion and potentiodynamic polarisation testing in an aerated 3.5 mol/l NaCl solution.

had peeled from the substrate before completion of the loading to 200 N – a conclusion confirmed by the SEM images of specimen A after the fretting test (Fig. 10).

Fig. 9 (b) shows the evolution of the COFs during the stabilization period of reciprocating sliding tests of B specimens taken before (B_1) and after (B_2) electrochemical investigation. The COF for specimen B_1 shows some mild step-like variations, particularly at early times, but the COF remained <0.07 throughout the whole fretting test (i.e. for 36,000 s, 300,000 cycles) – consistent with the absence of any obvious flaking-off of this diamond film in the SEM image shown in Fig. 11. A different COF versus time variation was observed for specimen B_2 . The COF in this case is relatively higher at early time (i.e. before 5000 s, 42,000 cycles), and then increases suddenly to >0.30 after $\sim 68,000$ cycles – indicating that the diamond film flaked off at this time. Once again, such conclusions are backed up by SEM analysis (Fig. 12).

Physically, rougher surfaces can cause increased ploughing and hence higher friction. The high COFs of the rough diamond film surface can be attributed to the abrasive cutting and ploughing effects of sharp asperities on the softer counterface of the Si_3N_4 ball. Thus the ploughing effects created by a diamond film on the counterface balls can be substantial, and reveal themselves as higher friction in the early stages. The present data suggests that the surface asperities are fractured or smoothed by repeated sliding passes during the run-in period, and that the magnitude of the microcutting and ploughing contribution to the friction therefore decreases with time (see Fig. 9). As the sliding test continues, the rough microcrystalline diamond films can be polished (see Fig. 10), and very low COFs are obtained when such polished films are used in sliding-contact experiments. Fig. 13 shows schematic wear tracks for the diamond films and the Si_3N_4 balls. In the early stages of a sliding test, the contact area (S) of the Si_3N_4 ball on the diamond film is very small (approximating point-contact), which makes the sliding test more like a scratch test under a large (200 N) load. As the sliding test progresses, the contact area of the Si_3N_4 ball on the diamond film (both the width (w) and the depth (h)) will increase continuously (as illustrated in Fig. 13) and new asperities

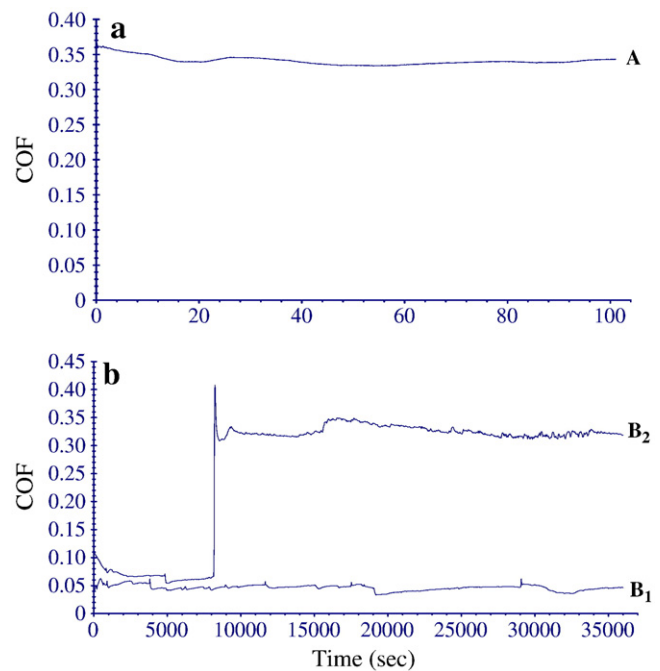


Fig. 9. Evolution of the friction coefficient of Si_3N_4 balls sliding against diamond films on specimen A, and on B specimens taken both before (B_1) and after (B_2) electrochemical investigation. The measurement involved reciprocating sliding tests, performed in ambient air, with a load of 200 N and no added lubricant.

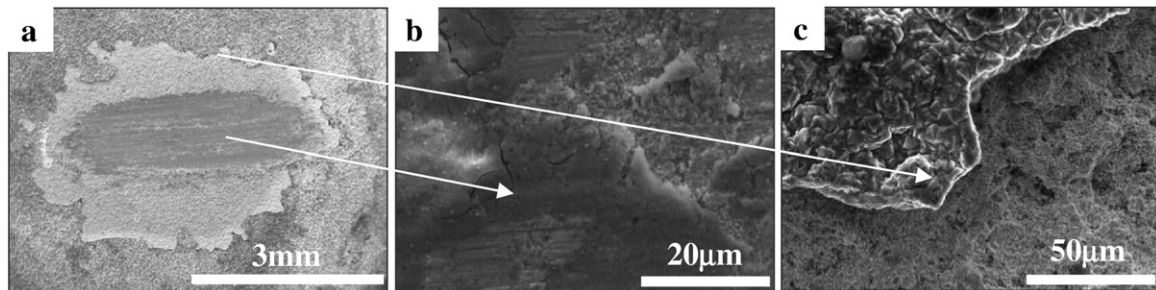


Fig. 10. SEM images of the sliding wear track on an A specimen.

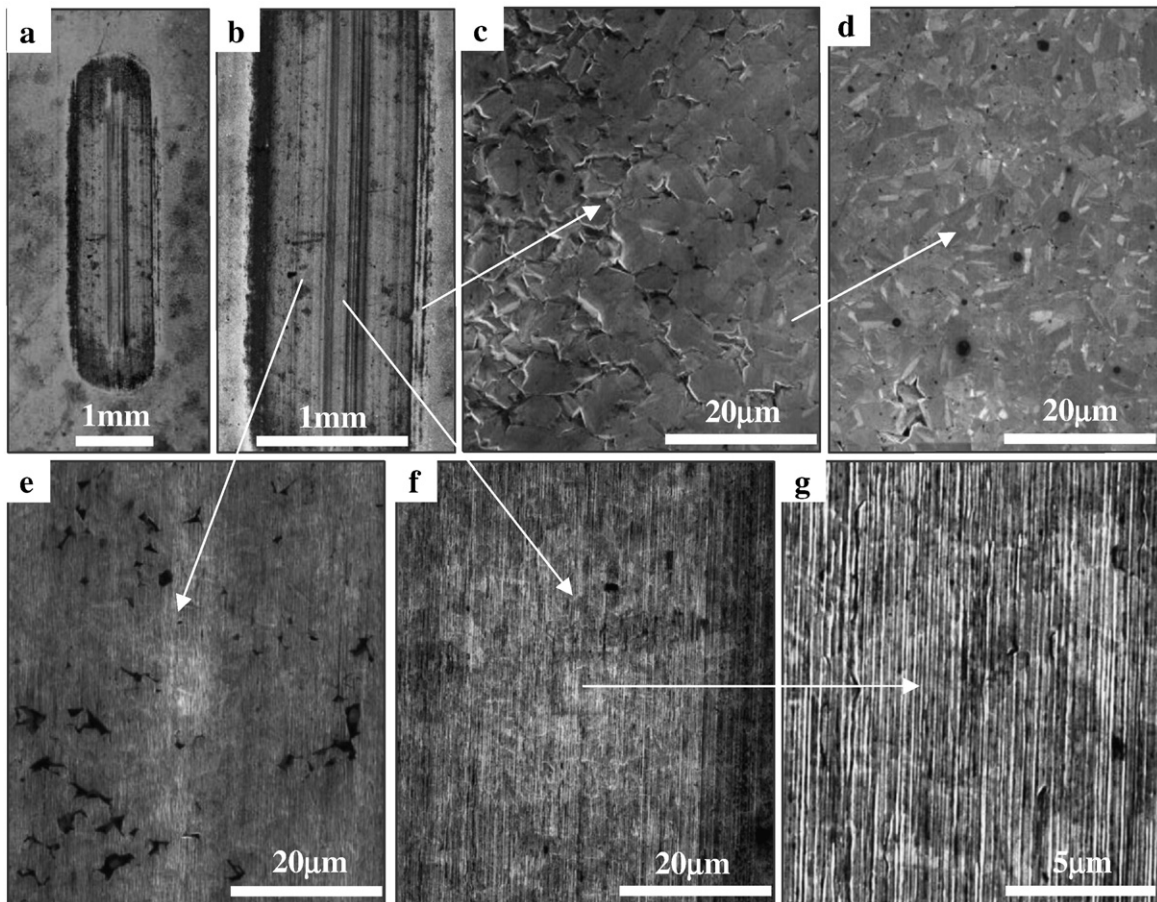


Fig. 11. SEM images of the sliding wear track on a B₁ specimen without electrochemical investigation. Image (a) shows the whole sliding wear track, while images (b)–(g) show selected portions of the wear track at higher magnification. The images were taken after sliding wear testing and ultrasonic cleaning with absolute ethyl alcohol.

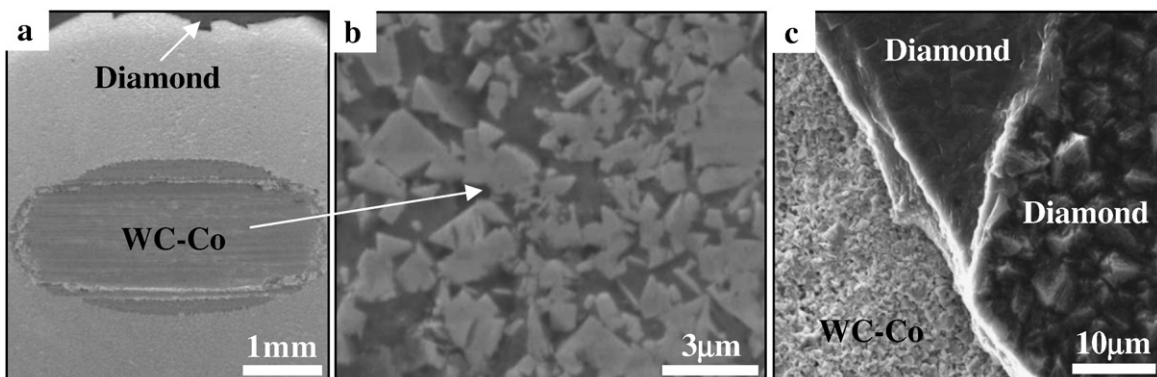


Fig. 12. SEM images of the sliding wear track on a B₂ specimen (*i.e.* after electrochemical investigation).

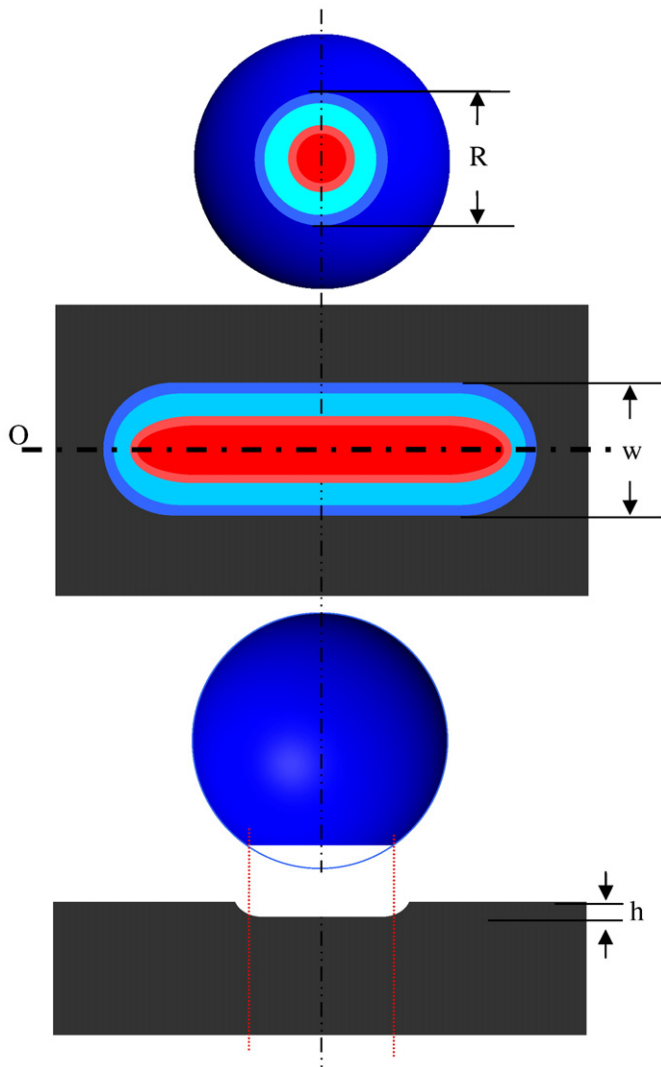


Fig. 13. Schematic illustration of the evolving wear track on a diamond film and a Si_3N_4 ball.

on the film surface will come into play, and then be progressively polished. The normal direction of the sliding trace will experience a longer wear-in period and heavier wear than that of the peripheral zone of the sliding trace (see Figs. 11 and 12). The pressure P between the diamond film and the Si_3N_4 ball will increase continuously, according to the equation $P = F \cdot S$ (where F represents the load), which will tend to increase the total shear force on the diamond film. When the total shear force exceeds the bond strength between the

diamond film and the WC–Co interlayer, the diamond film will flake off (see Fig. 9 (b)). Such flaking-off also demonstrates that the electrochemical corrosion testing reduces the adhesion of the diamond film. The XRD and cross-sectional morphology studies reveal that the diamond films have a columnar microstructure and a fibrous texture [23]. The NaCl solution might thus be expected to penetrate into the WC–Co/diamond film interface through the columnar structures and the intercrystallite pores, encouraging corrosion of WC–Co at the interface and reducing adhesion at the interface between the diamond film and the WC–Co interlayer.

3.7. Investigations of the substrate/interlayer interface

Rockwell indentation tests performed with total loads of, respectively, 600 N and 1500 N on a B_2 specimen after the diamond film had flaked off during reciprocating sliding tests (*i.e.* on a B sample after electrochemical investigation) confirm that the adhesion at the substrate/interlayer interface is still very good (see Fig. 14). Fig. 15 shows the compositional variation determined by EDX line scan analysis at this interface, before and after deposition of a diamond film. Diffusion of cobalt binder from the interlayer to the substrate is obvious following exposure to the high T_s involved in diamond deposition. The coefficient of thermal expansion of carbon steel is much higher than that of the WC–Co interlayer, so the interatomic spacings and the amplitudes of atomic vibration within the steel substrate increase more at elevated T_s than those of the WC–Co interlayer. Long growth times will allow the cobalt binder to diffuse further, even to the substrate surface given the Co concentration gradient, which will enhance adhesion at the substrate/interlayer interface.

4. Discussion

The various data sets, and the insights they provide regarding the deposited material and the diamond/interlayer and interlayer/steel interfaces, have already been discussed in the preceding sections and we here concentrate attention on the potential utility of such WC–Co interlayers in the production of diamond-coated steel tools.

During thermal spraying, the cobalt phase in a WC–Co particle starts to melt as it is heated in the hot gas jet and the WC grains begin to dissolve within it. The periphery of the semi-molten particle becomes decarburized by oxidation, promoting further WC dissolution. The molten or semi-molten particles then impact on the substrate to form a lamellar coating composed of many layers, called 'splats'. Particle quenching on impact with the substrate results in precipitation from the melt of W_2C and, possibly, W depending on the local melt composition – as demonstrated by the XRD data shown in Fig. 1 (a) [16]. Thermal spray coatings normally also contain non-uniform distributions of carbide and cobalt 'lakes'. The tribological

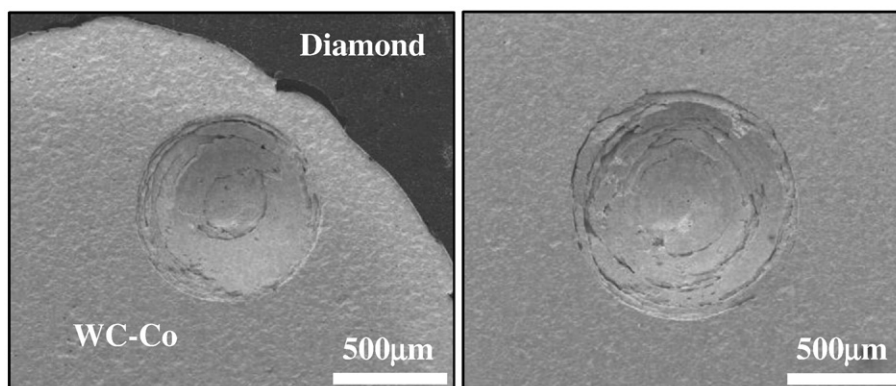


Fig. 14. SEM images of Rockwell indentations (600 N and 1500 N loads, respectively) of a B_2 specimen after the diamond film had peeled during fretting testing.

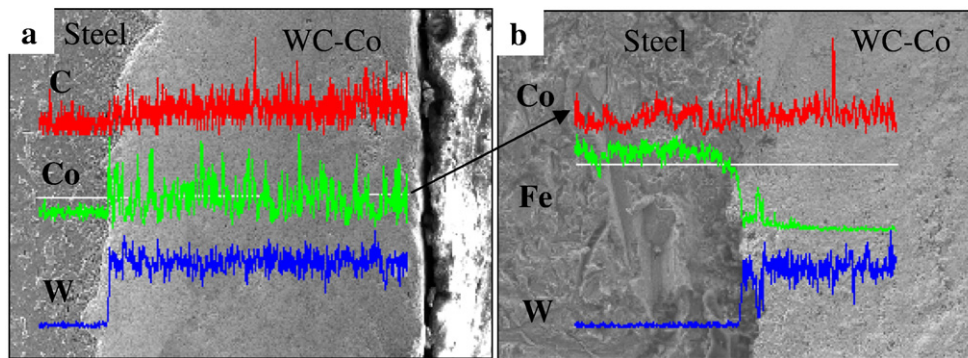


Fig. 15. Cross-sectional SEM images together with (superposed) EDX line scan analyses of the substrate/interlayer interface in a B₂ specimen (a) before and (b) after diamond film deposition.

behaviour, and the abrasion and erosion resistance of these thermally sprayed WC–Co coatings are generally poorer than that of bulk sintered WC–Co – reflecting the inhomogeneous microstructure and the phase transformations of the starting material, which can lead to wide variations in mechanical properties and in corrosion resistance [24]. Thakare et al. [25] identified preferential corrosion along the periphery of the carbide grain, *i.e.* in regions which are likely to have formed W₂C, and corrosion of the decarburized surface of the grain (which gradually progresses towards the carbide grain centre). Lima et al. [26] find that an increasing W₂C fraction is probably the most significant factor in reducing the fracture toughness of WC–Co coatings, and that appropriate post-heat treatments can improve the indentation toughness of thermally sprayed WC–Co coatings. Processing such thermally sprayed WC–Co coatings in a CH₄/H₂ atmosphere under diamond CVD conditions (*i.e.* high T_s) is very much like a uniform heat treatment. Diffusion of active atomic carbon encourages the transformation W₂C → WC, while Co diffusion tends to homogenize the microstructure and phase composition, with the result that the WC–Co interlayer develops a similar microstructure and phase composition to that of bulk sintered WC–Co (see Fig. 1), and the mechanical properties and corrosion resistance of the interlayer are enhanced.

No damage was observed on the diamond film surface in the present work after 300,000 sliding cycles under a large (200 N) load – a finding that accords with the results of the Rockwell indentation tests (see Fig. 6). These results clearly demonstrate that the diamond films on the B₁ specimens can impart very low COFs and low wear rates to sliding Si₃N₄ surfaces in open air. Such exceptional wear resistance is primarily attributed to the high mechanical strength and hardness of the diamond films. The present study demonstrates that WC–Co coatings can be the most effective interlayer, simultaneously guaranteeing diamond film quality and good adhesion at both the substrate/interlayer and the interlayer/diamond film interfaces.

5. Conclusions

A WC–Co coating prepared by high velocity oxy-fuel spraying has been used as an intermediate layer on carbon steel substrates to improve the quality and the nucleation density of diamond films and to enhance the diamond film adhesion. Reactive diffusion of atomic carbon during diamond film growth by CVD at high substrate temperatures in a CH₄/H₂ atmosphere causes the transformation W₂C → WC, while diffusion of cobalt binder from the interlayer to the substrate encourages some homogenization of the microstructure and phase composition. The WC–Co interlayer thereby develops a microstructure and phase composition similar to that of bulk sintered WC–Co. WC–Co coatings (after an appropriate chemical pretreatment) are shown to

constitute particularly good interlayers – which are efficient, cost-effective and simultaneously guarantee good adhesion at both the substrate/interlayer and interlayer/diamond interfaces. Diamond films can increase the electrochemical corrosion resistance of steel substrate in 3.5 mol/l NaCl solution, but such treatment degrades the film adhesion. The present study clearly demonstrates that diamond films deposited on steel substrates with a WC–Co interlayer have much to offer for future tribological applications. Unlike most other engineering materials, this composite coating material offers a combination of low friction, high hardness, and high wear and corrosion resistance.

Acknowledgements

The authors wish to thank the “China Scholarship Council”, the “State Key Laboratory of Powder Metallurgy”, the “Outstanding PhD Students Enabling Fund”, the “Innovation Foundation for Postgraduates of Hunan Province of China”, and the “Open Fund for Valuable Instruments of Central South University” for financial support.

References

- [1] P.K. Bachmann, *Adv. Mater.* 2 (1990) 195.
- [2] M.N.R. Ashfold, P.W. May, C.A. Rego, N.M. Everitt, *Chem. Soc. Rev.* 23 (1994) 21.
- [3] A. Bohner, R. Janisch, A. Hartmaier, *Scr. Mater.* 60 (2009) 504.
- [4] Y.S. Li, Q. Yang, C. Xiao, A. Hirose, *Thin Solid Films* 516 (2008) 3089.
- [5] Y.S. Li, A. Hirose, *Surf. Coat. Technol.* 202 (2007) 280.
- [6] N.G. Shang, C.H. Lee, X.T. Zhou, F.Y. Meng, C.Y. Chan, S.T. Lee, I. Bello, *J. Vac. Sci. Technol.* A19 (2001) 2968.
- [7] Y.S. Li, A. Hirose, *Chem. Phys. Lett.* 433 (2006) 150.
- [8] E. Nakamura, K.K. Hirakuri, M. Ohyama, G. Friedbacher, N. Mutsukura, *J. Appl. Phys.* 92 (2002) 3393.
- [9] R. Polini, G. Mattei, R. Valle, F. Casadei, *Thin Solid Films* 515 (2006) 1011.
- [10] K. Kellermann, C. Bareib, S.M. Rosiwal, R.F. Singer, *Adv. Eng. Mater.* 10 (2008) 657.
- [11] W.J.J. Van Enkevort, J.J. Schermer, J.G. Buijnsters, P. Shankar, J.J. Ter Meulen, US Patent, (2006) US77132129B2.
- [12] V.F. Neto, T. Shokuhfar, M.S.A. Oliveira, J. Grácio, N. Ali, *Int. J. Nanomanuf.* 2 (2008) 99.
- [13] R. Haubner, B. Lux, *Int. J. Refract. Met. H.* 24 (2006) 380.
- [14] H. Li, M. Gowri, J.J. Schenner, W.J.P. Van Enkevort, T. Kacsich, J.J. Ter Meulen, *Diamond Relat. Mater.* 16 (2007) 918.
- [15] Y.S. Li, Y. Tang, Q. Yang, C. Xiao, A. Hirose, *Int. J. Refract. Met. H.* 27 (2009) 417.
- [16] D.A. Stewart, P.H. Shipway, D.G. McCartney, *Acta Mater.* 48 (2000) 1593.
- [17] V.G. Ralchenko, A.A. Smolin, V.G. Pereverzev, E.D. Obratsova, K.G. Korotoushenko, V.I. Konov, Y.V. Lakhokin, E.N. Loubnin, *Diamond Relat. Mater.* 4 (1995) 754.
- [18] Q.P. Wei, Z.M. Yu, L. Ma, D.F. Yin, J. Ye, *Appl. Surf. Sci.* 256 (2009) 1322.
- [19] Z. Yu, U. Karlsson, A. Flodström, *Thin Solid Films* 342 (1999) 74.
- [20] S.M. Yang, Z.T. He, Q.T. Li, D.Z. Zhu, J.L. Gong, *Diamond Relat. Mater.* 17 (2008) 2075.
- [21] J.B. Donnet, D. Paulmier, H. Oulanti, T.L. Huu, *Carbon* 42 (2004) 2215.
- [22] V.F. Neto, R. Vaz, N. Ali, M.S.A. Oliveira, J. Grácio, *Diamond Relat. Mater.* 17 (2008) 1424.
- [23] P. Smereka, X. Li, G. Russo, D.J. Srolovitz, *Acta Mater.* 53 (2005) 1191.
- [24] R.J.K. Wood, *Int. J. Refract. Met. H.* 28 (2010) 82.
- [25] M.R. Thakare, J.A. Wharton, R.J.K. Wood, C. Menger, *Tribol. Int.* 41 (2008) 629.
- [26] M.M. Lima, J.C. Godoy, J.C. Avelar-Batista, P.J. Modenesi, *Mater. Sci. Eng.* A357 (2003) 337.